Human Molecular Genetics, 2015, Vol. 24, No. 7 1843–1855

doi: 10.1093/hmg/ddu602
Advance Access Publication Date: 1 December 2014
Original Article

ORIGINAL ARTICLE

SEPN1, an endoplasmic reticulum-localized selenoprotein linked to skeletal muscle pathology, counteracts hyperoxidation by means of redox-regulating SERCA2 pump activity

Marianna Marino[1,†], Tatiana Stoilova[1,†], Carlotta Giorgi[2], Angela Bachi[3], Angela Cattaneo[3], Alberto Auricchio[4], Paolo Pinton[2], and Ester Zito[1,*]

[1]Dulbecco Telethon Institute at IRCCS-Istituto di Ricerche Farmacologiche Mario Negri, Milan, Italy, [2]Section of Pathology, Oncology and Experimental Biology, Laboratory for Technologies of Advanced Therapies (LTTA), Department of Morphology, Surgery and Experimental Medicine, University of Ferrara, Ferrara, Italy, [3]IFOM-FIRC Institute of Molecular Oncology, Milan, Italy, and [4]Telethon Institute of Genetics and Medicine (TIGEM), Naples, and Medical Genetics, Department of Translational Medicine, Federico II University, Naples, Italy

*To whom correspondence should be addressed at: Dulbecco Telethon Assistant Scientist, IRCCS-Istituto di Ricerche Farmacologiche Mario Negri, Via La Masa 19, 20156 Milano, Italy. Tel: +39 0239014480; Fax: +39 023546277; Email: ester.zito@marionegri.it

Abstract

Selenoprotein N (SEPN1) is a broadly expressed resident protein of the endoplasmic reticulum (ER) whose loss-of-function inexplicably leads to human muscle disease. We found that SEPN1 levels parallel those of endoplamic reticulum oxidoreductin 1 (ERO1), an ER protein thiol oxidase, and that SEPN1's redox activity defends the ER from ERO1-generated peroxides. Moreover, we have defined the redox-regulated interactome of SEPN1 and identified the ER calcium import SERCA2 pump as a redox-partner of SEPN1. SEPN1 enhances SERCA2 activity by reducing luminal cysteines that are hyperoxidized by ERO1-generated peroxides. Cells lacking SEPN1 are hypersensitive to ERO1 overexpression and conspicuously defective in ER calcium re-uptake. After being muscle-transduced with an adeno-associated virus driving ERO1α, SEPN1 knockout mice unmasks a myopathy that resembles the dense core disease due to human mutations in *SEPN1*, whereas the combined attenuation of ERO1α and SEPN1 enhances cell fitness. These observations reveal the involvement of SEPN1 in ER redox and calcium homeostasis and that an ERO1 inhibitor, restoring redox-dependent calcium homeostasis, may ameliorate the myopathy of SEPN1 deficiency.

Introduction

SEPN1, a member of the selenocysteine-containing protein family, is localized in the ER lumen, ubiquitously expressed throughout the body, and of unknown function (1,2). Despite its wide expression, SEPN1 mutations give rise to a selective muscle phenotype that suggests the interaction of SEPN1 with proteins involved in muscle physiology (3,4).

Many selenocysteine-containing proteins are enzymes involved in oxidation–reduction reactions whose selenocysteine residue is usually located in the catalytic site because its nucleophilicity induces strong enzymatic activity (5). Like other members of the family, SEPN1 is also thought to have a redox function, and this idea is supported by the observation of a motif similar to the catalytic site of thioredoxin reductases (TRs) on the ER side of the

[†]These authors contributed equally to the study.

Received: October 7, 2014. **Revised and Accepted:** November 26, 2014

SEPN1 sequence. In agreement, excessive protein oxidation in cells devoid of SEPN1 has been observed (1,6,7).

Calcium homeostasis has a crucial function in muscle and depends on the redox status of both cytoplasmic and luminal cysteines in calcium-handling proteins (8,9). Among the calcium-handling proteins of the ER the Ca^{2+}-ATPase (SERCA) pumps have the highest affinity for Ca^{2+} removal from the cytosol and therefore determine the resting cytosolic Ca^{2+} concentration which is important in the process of excitation–contraction coupling. Three differentially expressed genes encode at least five isoforms of the SERCA pump. SERCA1a and 1b are expressed in fast twitch muscle fibers of skeletal muscle, SERCA3 has limited expression in various non-muscle tissues, whereas SERCA2a is expressed in slow-twitch fibers of skeletal muscle and in cardiac muscle. Its C-terminally extended isoform SERCA2b is ubiquitously expressed in muscle and non-muscle tissues (10). Interestingly, cysteine-dependent interactions between the oxidoreductase ERp57 and the fourth luminal loop of the SERCA2b inhibit calcium reuptake into the ER by oxidizing two cysteines in the L4 of this ATP-driven pump (11).

ER oxidoreductin 1 (ERO1) is the main ER protein disulfide oxidase that channels electrons from PDI to the terminal acceptor of electrons in the reaction: i.e. molecular oxygen, which is reduced to H_2O_2 (12–14). The oxidative activity of ERO1 may therefore burden the cell with potentially toxic reactive oxygen species (ROS) (15,16).

ERO1 transcription is activated by the unfolded protein response (UPR), which is one of the primary processes triggered by altered environmental cues in skeletal muscle, and contracting skeletal muscle produces ROS which, if they are not metabolized, can cause oxidative damage to the macromolecules in muscle fibres (17–20).

Therefore, ROS production by increased ERO1 expression in a contracting muscle may be harmful and be responsible for the maladaptive branch of the UPR (21).

Consistent with this idea, a partial decrease in ERO1 activity is compatible with life and promotes resistance to the lethal effects of high ER stress levels, which suggests that less ERO1 may be an advantage under some unusual conditions (22–24).

Given that muscle activity begets ER stress and enhances ERO1 activity with an attendant ER-localized peroxide production, and that ER thiol redox plays a crucial role in calcium homeostasis, we examined the possibility that the loss of an SEPN1-mediated reductive function leads to myopathy exposing cells to an H_2O_2-mediated hyperoxidation of key molecules involved in calcium handling.

We therefore established an unbiased method for uncovering redox-substrates of SEPN1 and found SERCA2 as one of them.

Results

SEPN1 protects against the hyperoxidizing conditions elicited by ERO1

SEPN1 mutant cells are more sensitive to oxidative stress and show excessive protein oxidation (6), so we followed SEPN1 expression in cells transfected with ERO1α, one of the main protein disulfide oxidases whose H_2O_2-generating activity can lead to ER hyperoxidation/misoxidation. Immunoblotting of protein lysates from HEK 293T cells transfected with ERO1α and harvested at different times showed that SEPN1 induction paralleled the level of ERO1α overexpression (Fig. 1A, lanes 1–4).

The treatment of cells with tunicamycin and thapsigargin, two inducers of ER stress, elicits the adaptive UPR and the

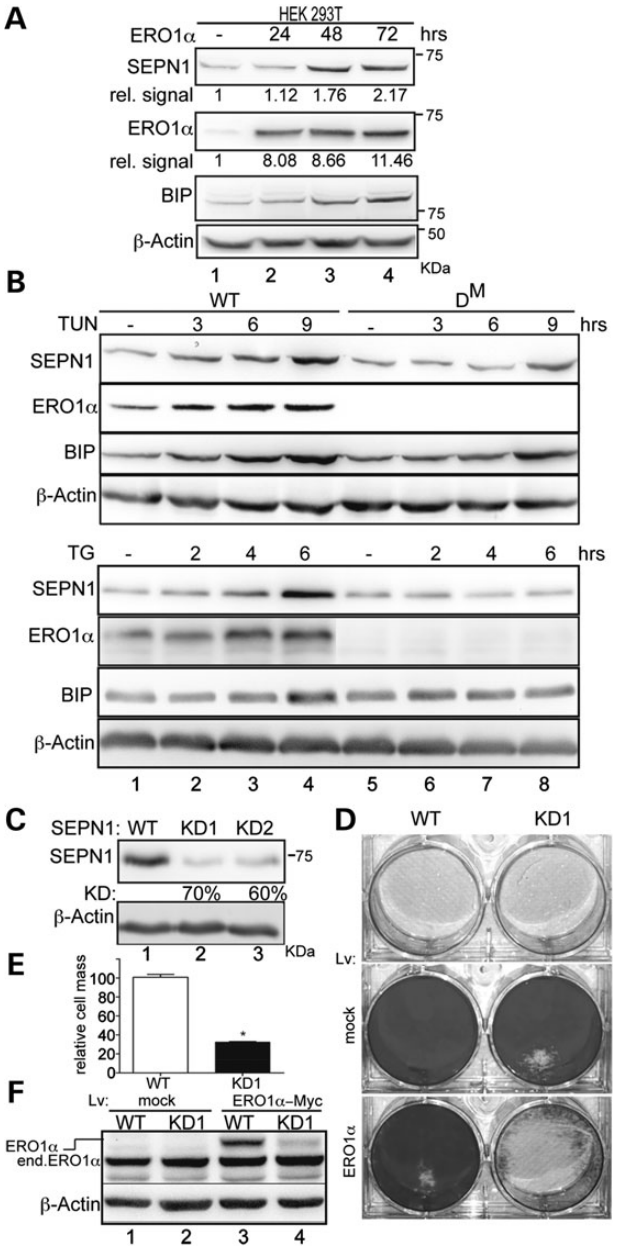

Figure 1. SEPN1 protects against the hyperoxidizing conditions elicited by ERO1 induction. (**A**) Immunoblot of SEPN1, ERO1α, BIP and β-actin in extracts of HEK-293T transfected with *ERO1α* and harvested at different time points. The relative amount (rel.signal) of SEPN1 and ERO1 is entered under the immunoblot and expressed as arbitrary units (a.u.) of the ratio of SEPN1 and ERO1 to the β-actin signal. (**B**) Immunoblots of SEPN1, ERO1α, BIP and β-actin from WT and D^M (double mutant for ERO1-α and ERO1-β) MEFs treated with 0.5 ug/ml tunicamycin (TUN) or 0.5 mM thapsigargin (TG) for different times. (**C**) Immunoblot of SEPN1 and β-actin in C2C12 7 days after transduction with a *puro*^{r}-marked lentivirus carrying an irrelevant insert (WT) or two different short hairpin RNAs directed to mouse SEPN1: KD1 and KD2. The relative percentage of knockdown SEPN1 (KD) is specified beneath the blot. (**D**) Photomicrographs of crystal violet-stained WT and KD1 C2C12 cells untransduced (unt.) or transduced with a blasticidin resistance-marked lentivirus expressing green fluorescent protein (GFP, indicated as mock) or ERO1α-Myc. (**E**) As in "D": quantification of cell mass after the transduction of WT and KD1 C2C12 cells with the mock *GFP* lentivirus (set at 100%) or the *ERO1α-Myc* lentivirus followed by blasticidin selection for 7 days (mean values and SEM, $n = 3$, $^*P < 0.01$). (**F**) Immunoblot of ERO1α and β-actin from WT and KD1 C2C12 cells after transduction with a blasticidin resistance-marked lentivirus expressing either *GFP* or *ERO1α-Myc* showing endogenous ERO1α (end. ERO1α) and slowly migrating ERO1α-Myc (ERO1α).

consequent up-regulation of ERO1 in order to increase cell survival (21). However, in certain circumstances of ER-stress a partial loss of function of the essential ERO1 gene enhances the ability of yeasts and worms to cope with severe stress as it burdens the cells with less H_2O_2 (23,24). Gene duplication events in vertebrates have generated two ERO1 isoforms, ERO1α and ERO1β, and mice with strong hypomorphic mutations in both ERO1s (D^M mice) are viable (25). SEPN1 induction by tunicamycin and thapsigargin was less in D^M mouse embryonic fibroblasts (MEFs), thus indicating that SEPN1 induction is attenuated in cells lacking ERO1 (Fig. 1B compare lanes 1–4 with 5–8) and suggesting a co-regulation of SEPN1 and ERO1.

In order to test the effect of ERO1 activity in SEPN1-deficient cells, we stably lowered SEPN1 gene products by means of lentiviral RNAi in C2C12 cells, a myoblast mouse cell line that expresses high levels of SEPN1. The resulting pools of KD1- and KD2-infected cells had, respectively, 70 and 60% lower SEPN1 levels (Fig. 1C, lanes 1–3), so we used the SEPN1 KD1 cells for the subsequent experiments. Lentiviral vectors carrying a dominant selection marker that imparts blasticidine resistance were used to transduce ERO1α-Myc in wild-type (WT) and KD1 cells, and led to the growth of a thick carpet of ERO1α-transduced WT cells, but the transduction of ERO1α in KD1 cells failed to elicit the growth of blasticidine-resistant colonies (Fig. 1D and E), and the few cells recovered had a low level of transduced ERO1α (Fig. 1F, lanes 3 and 4), indicating that low levels of SEPN1 are incompatible with high levels of ERO1α.

High cysteinyl sulfenic acid levels in SEPN1 knockdown cells

ERO1 is a key enzyme in oxidative protein folding whose oxidative activity is related to the build-up of H_2O_2 (16).

Remarkably, the build-up of H_2O_2 inside the ER exposes the free thiols of new client proteins to competing H_2O_2-mediated oxidation, which leads to an increase in sulfenylated proteins; these can be transient intermediates in the formation of more stable disulfides, or upon a further burst of H_2O_2, trapped in an irreversible state of higher oxidized sulfur oxides (26).

In order to compare the burden of sulfenylated proteins in freshly lentiviral-infected C2C12 cells with different levels of SEPN1, we exposed the cells and lysates to dimedone, a chemical that selectively modifies sulfenylated cysteines, and detected the dimedone-modified proteins by means of immunoblotting using an antibody against the chemically modified group (27). In the absence of dimedone, the antibody gave a weak background signal (Fig. 2A, lane 4) but, importantly, the sulfenic acid signal was considerably stronger in the KD1 cells and in cells overexpressing ERO1α, both of which showed a discrete band of ~110 kDa (Fig. 2A, lanes 1 and 3). On the contrary, SEPN1 knockdown had no effect on the redox state of the sentinel ER-localized reduction–oxidation sensitive green fluorescent protein (roGFP-iE) (Fig. 2B lanes 1 and 2) (28,29).

Glutathione is the main scavenger of cellular H_2O_2 and acts to protect the ER from hyperoxidizing conditions (30,31). Since it has been shown that hyperactive ERO1 and the direct exposure to H_2O_2 inside the ER increases luminal oxidized glutathione levels, we tested the level of total and oxidized glutathione in WT and KD1 cells (32,33). The 1.5-fold increase in the oxidized to total glutathione ratio in the KD1 cells was consistent with an H_2O_2-mediated hyperoxidation that was not compensated by SEPN1 (Fig. 2C).

An SEPN1-trapping mutant engages protein-substrates in an ERO1-dependent manner

As human SEPN1 has a domain (CU: C427, U428) resembling the active site of TR, we took advantage of the electron transfer

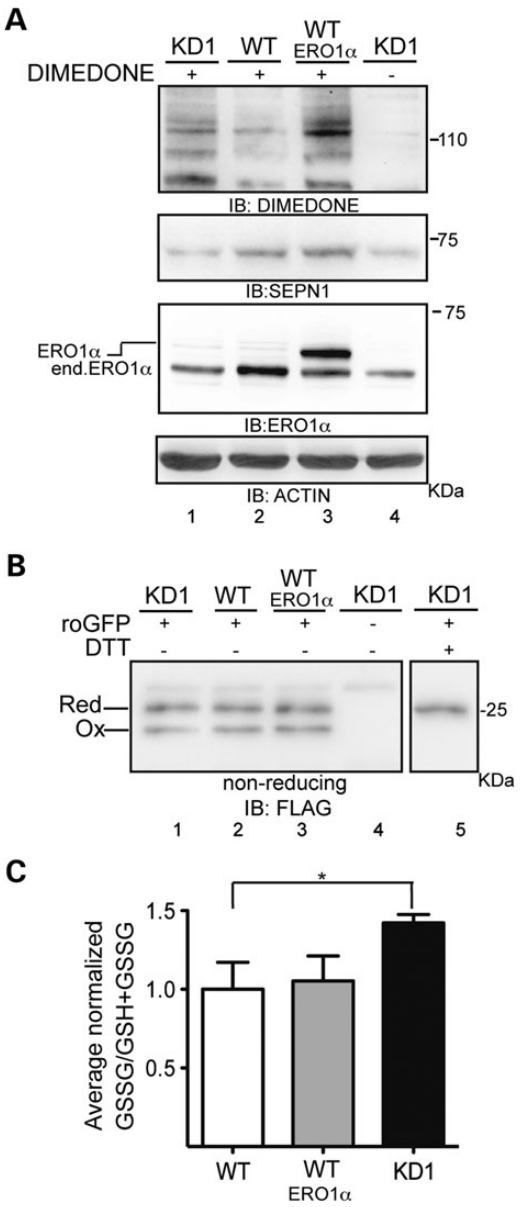

Figure 2. High cysteinyl sulfenic acid levels in SEPN1 knockdown cells. (**A**) Immunoblots of extracts from KD1, WT and WT transduced with *ERO1α* C2C12 cells exposed to the sulfenic acid-reactive probe dimedone and an antibody reactive to dimedone-conjugated cysteine residues. The immunoblot of β-actin is shown as the loading control. (**B**) Immunoblot of FLAG_M1_roGFP_iE immunopurified from the ER of cells with the indicated genotypes. The purified proteins were resolved by SDS–PAGE under non-reducing conditions. The position of the reduced and oxidized FLAG_M1_roGFP_iE in a typical experiment is shown. (**C**) Bar diagram of the ratio between oxidized glutathione (GSSG) to total glutathione (GSH + GSSG) content in cells of the indicated genotypes. Results are normalized to the control WT and are the mean of three independent experiments ($n = 3$, $^*P < 0.01$).

mechanism of TR to identify the redox-mediated substrates of SEPN1. Mammalian TRs have a C-terminal redox-active tetrapeptide (GCUG) in which the cysteine-selenocysteine dyad represents the active site. The enzymatic mechanism of TR relies on an exchange of electrons with the thioredoxin (Trx) substrate: the nucleophilic selenolate anion of selenocysteine attacks a (sulfenylatable) cysteine on Trx to form a selenenylsulfide intermediate that is later resolved by the cysteine in the redox-active motif of TR (34,35).

Based on this mechanism, we generated an SEPN1 mutant devoid of the resolving cysteine (C427, which was mutated to serine) in order to trap the redox substrates of SEPN1 (Fig. 3A). To overcome the low level of SEPN1 expression due to the presence of the selenocysteine (U428), this residue was converted to the similar cysteine amino acid (Fig. 3B). This modification is supported by the fact that a previous study using a cysteine- or selenocysteine-based trapping mutant of TR did not reveal any difference between the interactors of the two enzyme forms (36).

In order to establish the system of SEPN1-SC-pFLAG (the trapping mutant of SEPN1) and SEPN1-SS-pFLAG (a potential redox negative control lacking U and C), the proteins were expressed by means of the transient transfection of HEK 293T cells. The localization of SEPN1-SC-pFLAG and SEPN1-SS-pFLAG was first checked by means of indirect immunofluorescence which, as expected, showed that both co-localize with PDI in the ER (Fig. 3C).

We then prepared protein lysates from *SEPN1-SC-pFLAG*- and *SEPN1-SS-pFLAG*-transfected cells in the presence of *N*-ethylmaleimide (NEM) in order to quench the free thiols, and the protein complexes were immunopurified using the FLAG-M2 tag. Immunoblotting of the non-reducing gel showed two main bands of ~70 and 140 kDa, probably corresponding to monomers and covalent homodimers of SEPN1, and additional bands in a high-molecular disulfide-bonded complex associated exclusively with SEPN1-SC-pFLAG and representing potential client proteins (Fig. 3D, lanes 2 and 4). The simultaneous overexpression of ERO1α made the appearance of these bands more conspicuous, probably by enhancing the interaction between SEPN1-SC-pFLAG and the clients (Fig. 3D, lanes 1 and 2). On the contrary, the delivery of a catalase–peroxidase to the ER made these bands less conspicuous (Supplementary Material, Fig. S1, compare lane 1 with 2). These observations confirmed that the trapping mutant was useful for identifying the redox-regulated interactors of SEPN1 and that SEPN1 interacts with these in an H_2O_2-dependent manner.

An SEPN1-trapping mutant forms a stable complex with SERCA2

In order to identify the protein(s) that may be associated with the trapping mutant of SEPN1 in a disulfide-bonded complex, we excised the region of the non-reducing SDS–PAGE containing the trapped complexes. Following gel reduction, alkylation and digestion with trypsin, the peptides eluted from the gel slices were analyzed by means of LC–MS-MS (Fig. 4A), and the corresponding human proteins were sorted and scored by means of label-free quantification (Fig. 4B). Among the ER proteins discovered in a disulfide complex exclusively with the SEPN1-trapping mutant (and not with SEPN1-SS-pFLAG), we focused our attention on the ER calcium pump SERCA2 because of its pivotal role in calcium signalling.

The excitation–contraction coupling that connects membrane depolarization with cytosolic calcium concentration and cell shortening is fundamental for muscle physiology. An action potential on neuromuscular junctions triggers a series of events that culminate in the SERCA-mediated re-uptake of Ca^{2+} into the ER/SR (sarcoplasmic reticulum), which brings cytosolic calcium to the resting level of muscle relaxation (37). The SERCA family includes various gene products and related splicing variants that are all involved in SR/ER calcium uptake. Importantly, SERCA2b is ubiquitously expressed in muscle and non-muscle tissues and whose activity depends on the redox status of two cysteines exposed in the lumen of the ER (11). SERCA2a is the main isoform of SERCA in slow-twitch muscle fibres (and models

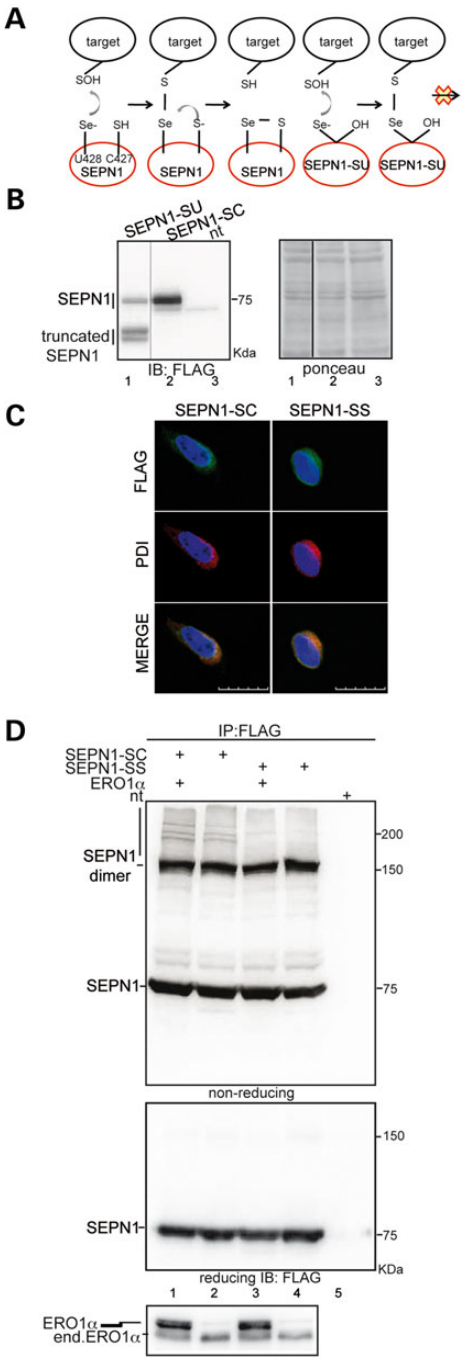

Figure 3. An SEPN1-trapping mutant engages protein-substrates in an ERO1-dependent manner. (**A**) Proposed catalytic mechanism of mammalian SEPN1. The sulfenylated substrate (SOH) accepts electrons directly from the selenolate anion (U428) of SEPN1, and the intermediate selenenylsulfide bond formed between SEPN1 and the substrates is resolved by the cysteine (C427). The substrate could be trapped in a complex with a mutant SEPN1 (SEPN1-SU) lacking the resolving cysteine (C427) (that is mutated to serine) of its active C-terminal site. (**B**) Immunoblot of Flag-tagged SEPN1-SU and SEPN1-SC transfected in HEK-293T cells. The truncated SEPN1-SU is due to the UGA codon of the selenocysteine that is recognized as a stop codon. (**C**) Immunostaining of PDI and Flag-tagged SEPN1-SC and SEPN1-SS transfected in HEK-293T cells (scale bar: 20 μm). (**D**) Non-reducing and reducing Flag immunoblot of Flag-M2 immunopurified proteins from HEK-293T cells transfected as indicated. The low mobility complex containing immunoreactive material in complex with SEPN1-SC is indicated by a vertical line. Bottom: ERO1α reducing immunoblot of proteins from transfected cells. Transfected ERO1α is distinguished from the endogenous form because of the Myc tag.

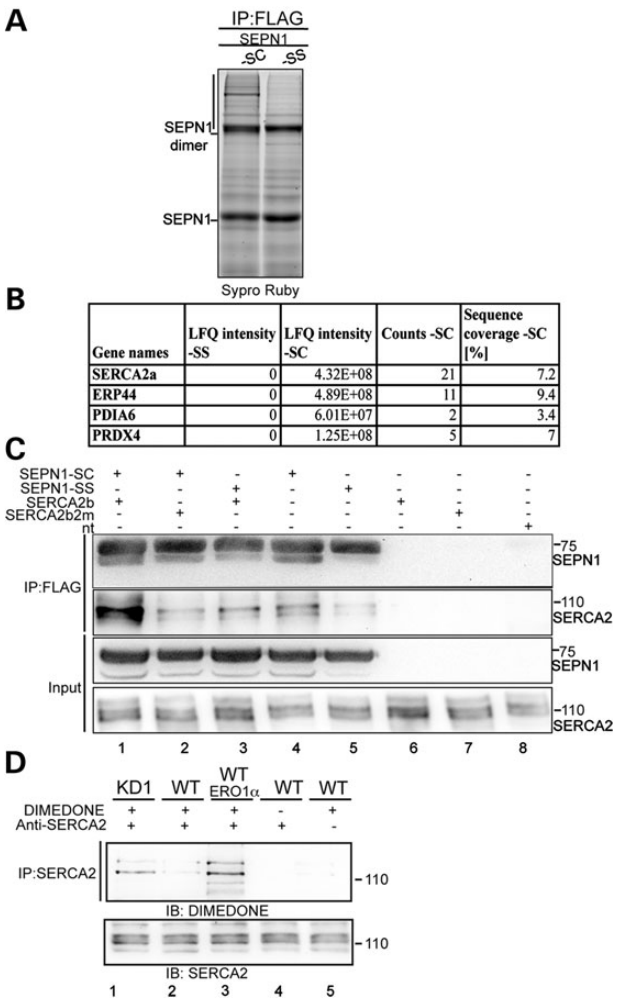

Gene names	LFQ intensity -SS	LFQ intensity -SC	Counts -SC	Sequence coverage -SC [%]
SERCA2a	0	4.32E+08	21	7.2
ERP44	0	4.89E+08	11	9.4
PDIA6	0	6.01E+07	2	3.4
PRDX4	0	1.25E+08	5	7

Figure 4. An SEPN1-trapping mutant forms a stable complex with SERCA2 in mammalian cells. (**A**) Sypro Ruby stained non-reducing SDS–PAGE of proteins immunopurified in complex with FLAG-tagged SEPN1-SC and SEPN1-SS. The vertical line demarcates the region analyzed by mass spectroscopy protein analysis. (**B**) List of proteins identified by means of LC–MS-MS sequencing of the tryptic peptide of endogenous proteins captured in disulfide-linked complex by a FLAG M2-tagged trapping mutant SEPN1-SC in HEK-293T cells. The ER proteins found only in SEPN1-SC were sorted against the total number of proteins using the Label Free Intensity parameter. (**C**) Anti-Flag and anti-SERCA2 immunoblots of proteins immunopurified with the FLAG-M2 antibody from lysates of HEK 293T cells that were untransfected or transfected with the indicated expression plasmids. The lower two panels show, respectively, 5 and 10% of the total lysates before IP ("Input"). The proteins shown were resolved by means of reducing SDS–PAGE. (**D**) Immunoblot using antibody reactive to dimedone-conjugated cysteine residues of the protein samples shown in Figure 2A immunopurified with SERCA2 antibody. The immunoblot made using SERCA2 antibody is shown at the bottom.

of SEPN1 loss of function show a selective hypotrophy of slow-twitch muscle fibres (38)) and contains the two exposed cysteines (10).

A substantial amount of endogenous SERCA2 immunoreactivity was found complexed with SEPN1-SC-pFLAG in HEK 293T cells (Fig. 4C, lane 4). In order to characterize the association between SEPN1-SC-pFLAG and SERCA2, the cells were transfected with various combinations of SEPN1-SC-pFLAG, SEPN1-SS-pFLAG, pig SERCA2b and the mutant pig SERCA2b2m which lacks the two cysteines (C875 and C887) in the L4 ER domain. The protein extracts were quenched with NEM and immunoprecipitated with FLAG M2; the immunocomplexes were resolved under reducing conditions, and the blots were decorated with anti-FLAG and anti-SERCA2. An abundant band corresponding to SERCA2 was detected in the sample co-transfected with SEPN1-SC-pFLAG and SERCA2b (Fig. 4C, lane 1). Of note, a much lower level of association was seen between SEPN1-SC-pFLAG and SERCA2b2 m (Fig. 4C, lane 2). A weak band corresponding to SERCA2 was detected in the samples co-transfected with SEPN1-SS-pFLAG and SERCA2b, as well as in the sample transfected with SEPN1-SS-pFLAG alone, thus indicating a weak non-covalent association between SEPN1SS and SERCA2 (Fig. 4C, compare lane 1 with 3 and lane 4 with 5). Because SERCA2a also contains the two cysteines (C875 and C887) in the L4 ER domain, we tested whether SEPN1-SC-pFLAG associates with SERCA2a through the cysteines in the L4 domain. We co-expressed SEPN1-SC-pFLAG and SERCA2a or SERCA2a2m which lacks the two cysteines (C875 and C887) and found that SEPN1-SC covalently associates also with SERCA2a through the cysteines in the L4 domain (Supplementary Material, Fig. S2, compare lane 1 with 2).

Hyperoxidized SERCA2 detected in cells devoid of SEPN1

As the molecular mass of all of the SERCA2 splicing variants is ~110 kDa, we investigated whether the most abundant dimedone-reactive protein in the KD1 cells and the cells overexpressing ERO1 corresponded to SERCA2 (Fig. 2A, lanes 1 and 3). To this end, protein lysates of C2C12 cells with different levels of SEPN1 and C2C12 cells overexpressing ERO1 were exposed to dimedone in order to quench the sulfenylated cysteines, and the proteins were immunopurified using an SERCA2 antibody. Immunoblotting SERCA2 and its related protein complex with an antibody against dimedone revealed a signal of ~110 kDa that suggested a sulfenylated SERCA2, the levels of which were higher in KD1 cells and in the cells overexpressing ERO1α (Fig. 4D, lanes 1 and 3).

Redox-active SEPN1 increases SERCA-dependent Ca^{2+} entry into the ER

Given the redox interaction between SEPN1 and SERCA2, and the redox-regulated activity of SERCA2, we analyzed the potential redox role of SEPN1 in SERCA-dependent Ca^{2+} entry using cells that were devoid of, or overexpressing SEPN1. Ca^{2+} levels and fluxes were monitored using an ER-targeted aequorin probe that allows the direct measurement of calcium in the ER, thus overcoming some of the uncertainties associated with indirect Ca^{2+} measurements and providing a significant advantage when investigating Ca^{2+} homeostasis in the ER. The reconstitution of active aequorin with coelenterazine in the ER lumen requires the previous depletion of Ca^{2+} from the organelle followed by refilling (39). Figure 5B shows that the re-addition of Ca^{2+} to the medium rapidly increases $[Ca^{2+}]$ levels within the ER ($[Ca^{2+}]_{ER}$) up to a steady-state level of ~500 μM (SEPN1: 508 ± 23 μM; SEPN1-SS: 510 ± 20 μM; $n = 10$) in HeLa cells transfected with the vector harbouring cDNA for SEPN1 (but not expressing the full-length SEPN1 protein because, in the absence of sodium selenite, the UGA codon of the selenocysteine is recognized as a stop codon, as shown in lane 2 of Fig. 5A), or for the mutant SEPN1-SS protein. Under the same conditions, the steady-state ER level after sodium selenite treatment in cells overexpressing SEPN1 was significantly higher (586 ± 18 μM $n = 10$; $P < 0.05$), thus indicating potentiated SERCA activity. In contrast, the steady-state ER level in the sodium selenite-treated cells overexpressing the SEPN1SS mutant was slightly lower (432 ± 55 μM, $n = 10$), thus suggesting the inability of the mutant to increase SERCA activity. A difference in intra-luminal $[Ca^{2+}]$ levels between the ER of

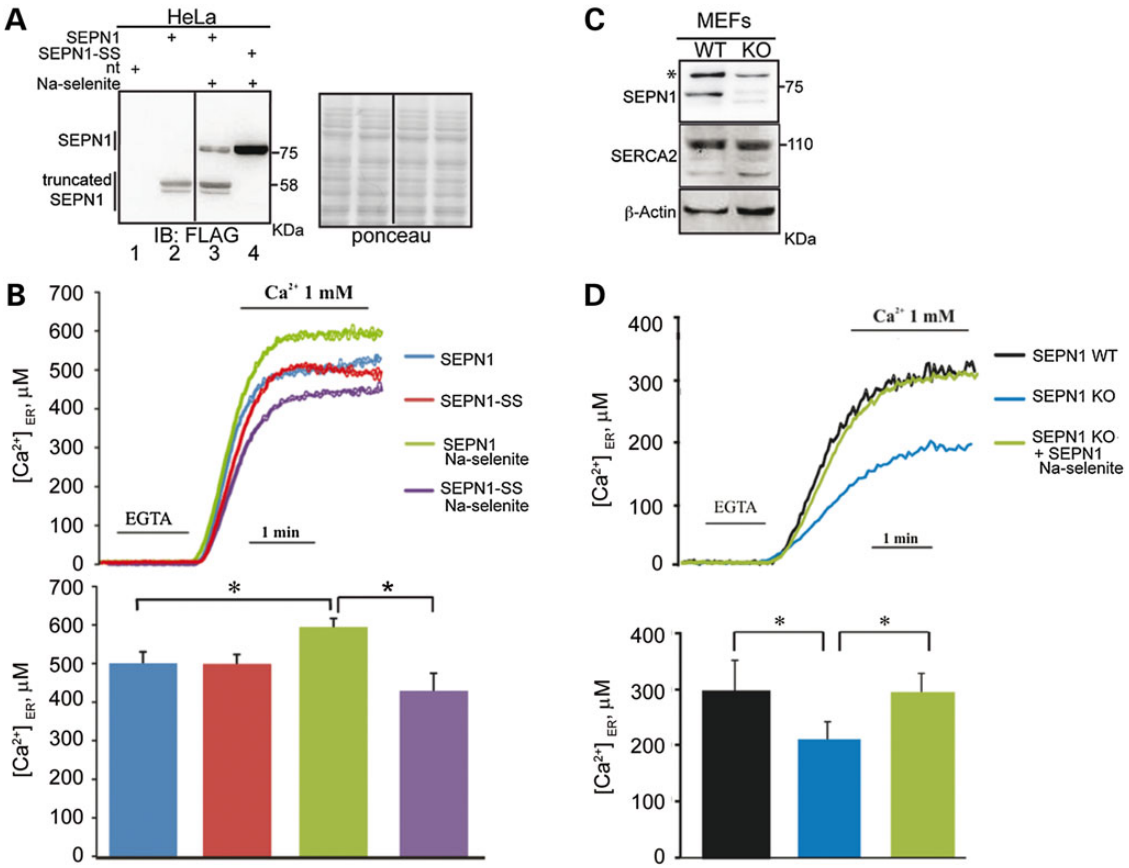

Figure 5. Reduced SERCA2 activity in freshly isolated SEPN1KO MEFs rescued by redox-active SEPN1. (**A**) Immunoblot of FLAG-tagged SEPN1 and SEPN1-SS transfected in HeLa cells in with or without Na-selenite. Note the truncated SEPN1 in the cells without Na-selenite. (**B**) HeLa cells were co-transfected with ER aequorin and SEPN1 or SEPN1-SS with or without Na-selenite, and calcium refilling of the ER was recorded. The trace is representative of 10 independent experiments that led to similar results. Bar graphs representing steady-state ER calcium levels are shown at the bottom ($n = 10$, $^*P < 0.05$). (**C**) Immunoblot of SEPN1 and SERCA2 from freshly isolated WT and SEPN1KO MEFs. * Background band. (**D**) Freshly isolated WT and SEPN1KO MEFs were co-transfected with ER aequorin and SEPN1 in the presence of Na-selenite, and calcium refilling of the ER was recorded. The trace is representative of eight independent experiments that led to similar results. Bar graphs representing steady-state ER calcium levels are shown at the bottom ($n = 8$, $^*P < 0.05$).

the cells expressing SEPN1 or SEPN1-SS was not only observed at steady-state but also in the maximal rate of Ca^{2+} accumulation in the ER (SEPN1: 18.86 ± 2.42 μM/s; SEPN1-SS: 13.96 ± 0.79 μM; $n = 10$) calculated at the beginning of ER Ca^{2+} refilling, i.e. when the rate is mainly dependent by the SERCA activity and neither influenced by ER Ca^{2+} leak nor by ER Ca^{2+} buffering.

We next examined SERCA activity in freshly isolated SEPN1 WT and SEPN1KO MEFs. As shown in Figure 5D, and in line with the results obtained in HeLa cells, the steady-state level of $[Ca^{2+}]_{ER}$ in the SEPN1 WT cells was ~300 μM, whereas it was lower in SEPN1KO MEFs (WT: 292 ± 50 μM; SEPN1KO: 189 ± 25 μM; $n = 8$; $P < 0.05$), and the rate of Ca^{2+} accumulation was also lower (WT: 3.6 ± 0.7 μM/s; SEPN1KO: 2.6 ± 0.5 μM/s; $n = 8$) despite comparable levels of SERCA2 (Fig. 5C). This alteration can be attributed to the absence of SEPN1 because the re-introduction of SEPN1 protein in SEPN1KO MEFs restored $[Ca^{2+}]_{ER}$ levels similar to those observed in WT cells (312 ± 47 μM; rate of accumulation 3.5 ± 0.7 μM/s; $n = 8$).

In line with a reductive function of SEPN1 that enhances SERCA activity by reducing the luminal H_2O_2-oxidized cysteines, the delivery of a catalase–peroxidase, but not a cognate catalase mutated in the active site, to the ER restored $[Ca^{2+}]_{ER}$ levels of SEPN1KO MEFs (Supplementary Material, Fig. S3).

As Ca^{2+} accumulation in the ER is determined by SERCA-dependent Ca^{2+} entry and Ca^{2+} efflux (most probably via inositol 1,4,5-trisphosphate receptors, IP3R1), we determined whether the lack of SEPN1 has some impact on Ca^{2+} efflux. Ca^{2+} efflux from the ER was compared in freshly isolated SEPN1KO MEFs and freshly isolated SEPN1WT MEFs after agonist stimulation of IP3R1. The SEPN1KO MEFs showed less SERCA activity, but there was no between-group difference in Ca^{2+} efflux suggesting that the activity of the major ER Ca^{2+} release channels IP3R1 was unaffected by SEPN1 protein (Supplementary Material, Fig. S4).

These results indicate that a redox-active SEPN1 regulates the calcium level of the ER potentiating SERCA activity by reducing the luminal H_2O_2-oxidized cysteines.

An ERO1 surge in the protected SEPN1 KO muscle reveals a myopathic phenotype

Unlike human and zebrafish, in which SEPN1 loss of function gives rise to an overt muscle phenotype, SEPN1KO mice are somehow protected, showing no gross alterations in muscle histology (3,4). This protection may be provided by the activity of redundant pathways controlling redox balance in mouse muscle and/or by the limited muscle activity.

We therefore decided to assess the effect of SEPN1 deficit in murine muscle forced into hyperoxidizing conditions by ERO1 overexpression.

In order to test the effects of ERO1 overexpression on the muscle phenotype of SEPN1KO mice, one-month-old WT and

SEPN1KO mice were given direct intramuscular injections of an AAV2/1-*ERO1α* vector in three sites of the right gastrocnemius muscle, and AAV2/1-*GFP* vector or vehicle alone was injected into the contralateral muscle. The animals were sacrificed 3 weeks after injection in order to allow sustained vector expression. The levels of ERO1α expression analyzed by means of western blotting were more than 10-fold higher in the AAV2.1- *ERO1α*-injected muscles than in the controls (Fig. 6A, compare lanes 1–4 with lanes 5–8).

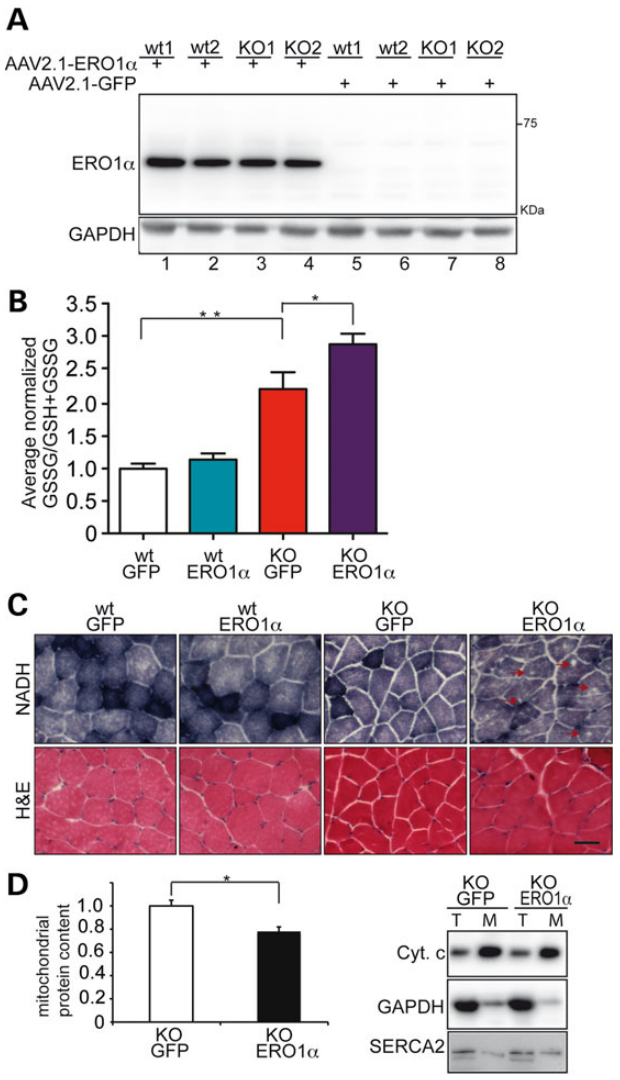

Figure 6. The intramuscular injection of AAV2.1-ERO1 in SEPN1KO mice promotes a myophatic phenotype. (**A**) ERO1α and GAPDH immunoblot of proteins extracted from the gastrocnemii of two WT and two SEPN1KO (KO) mice transduced with *AAV2.1-ERO1α* or *AAV2.1-GFP*. (**B**) Bar diagram of the ratio between oxidized glutathione (GSSG) to total glutathione (GSH+GSSG) content in *ERO1α*- and *GFP*-injected gastrocnemii of WT and SEPN1KO mice ($n = 5$, $^{*}P < 0.05$, $^{**}P < 0.01$). Results are normalized to the *GFP*-injected gastrocnemii of WT. (**C**) NADH and H&E staining of *ERO1α*- and *GFP*-injected gastrocnemii of WT and SEPN1KO mice. Serial sections of the gastrocnemius muscle were stained with H&E and NADH. Images with each stain were taken from the same area of the section, allowing the comparison of the same fibres with different staining methods (scale bar 100 μm). Red arrows indicate the myofibres that contain minicore lesions in NADH staining. (**D**) Bar diagram of the ratio between mitochondrial proteins to total proteins content in *ERO1α*- and *GFP*-injected gastrocnemii of SEPN1 KO mice. The ratio of the GFP-injected gastrocnemii was arbitrarily set at 1 ($n = 3$, $^{*}P < 0.01$). On the right: cythocrome c (cyt. c) (a mitochondrial protein), GAPDH (a cytosolic protein), SERCA2 (an SR protein), immunoblots of the total proteins (T) and enriched mitochondrial proteins (M).

In qualitative agreement with the cell-line results (Fig. 2B), 2- and 3-fold increases in the ratio of oxidized to total glutathione were, respectively, detected in the mock- and *ERO1α*-injected gastrocnemii of SEPN1KO, and could be attributed to an ERO1-mediated oxidative burst not counteracted by SEPN1 (Fig. 6B).

One of the most frequent pathological findings in patients with SEPN1 mutations is the presence of minicores, which correspond to areas of muscle that are depleted in mitochondria and characterized by a lack of staining of the mitochondrial enzyme NADH dehydrogenase (4). The presence of cores was investigated using NADH staining. As expected, the WT and SEPN1KO mouse muscles injected with vehicle alone or AAV2.1-*GFP* showed no abnormalities, but core lesions were observed in the gastrocnemius sections of the *ERO1α*-injected SEPN1KO mice (Fig. 6C). In order to quantify the loss of mitochondria, we isolated mitochondria from the gastrocnemii of the *GFP*- and *ERO1α*-injected SEPN1KO mice (Fig. 6D right panel), and measured the content of mitochondrial proteins. The ratio between the mitochondrial proteins and total protein content of the gastrocnemii indicated a 20% decrease in mitochondrial proteins in the *ERO1α* -injected SEPN1KO mice (Fig. 6D).

These observations indicate a physiological link between the reductase activity of SEPN1 and the oxidative power of ERO1.

Increased resistance to ER stress in cells with simultaneously attenuated SEPN1 and ERO1

In line with an ERO1-mediated oxidative insult that needs compensation and is not counteracted in cells devoid of SEPN1, the pool of C2C12 lentivirally infected with SEPN1 RNAi (KD1) showed slightly slower metabolic activity than their mock-infected counterparts. However, after 10 passages, the KD1 cells adapted to the cell culture conditions as reflected by their increased metabolic rate, which was also accompanied by a 70% decrease in ERO1 despite the normal levels of other ER markers (compare lanes 1 and 4 of (Fig. 7A and B) with lanes 1 and 2 of Fig. 1F). Moreover, the late-passage KD1 cells with less ERO1 were more resistant to the ER stress inducers tunicamycin and thapsigargin (Fig. 7B).

In order to investigate whether the resistance to ER stress was due to the lack of ERO1 or a pleiotropic effect of cell adaptation, freshly isolated SEPN1KO MEFs were treated with low concentrations of EN460, an ERO1 inhibitor. Remarkably, the cells devoid of SEPN1 and treated with EN460 (which traps ERO1 in a reduced state by blocking its enzymatic activity (Fig. 7C bottom)) were protected from exposure to tunicamycin (Fig. 7C). However, the protection was relatively modest as it was probably limited by toxicity due to the previously described non-selective reactivity of the ERO1 inhibitor (40). Nonetheless, these observations suggest the potentially protective role of ERO1 attenuation against the consequences of SEPN1 loss of function.

Discussion

Loss-of-function mutations in the human *SEPN1* gene are involved in early-onset recessive neuromuscular disorders known as SEPN1-related myopathies. The mechanisms behind these pathologies are poorly understood as the function of SEPN1 is still not known. Hence, the characterization of SEPN1 function and interactome would open up avenues of investigation for the design of suitable therapeutic approaches. The findings of this study show that SEPN1 can act as a reductase in the lumen of the ER (Fig. 3). Among the potential redox-regulated SEPN1 substrates, we identify SERCA2 isoforms (SERCA2a and

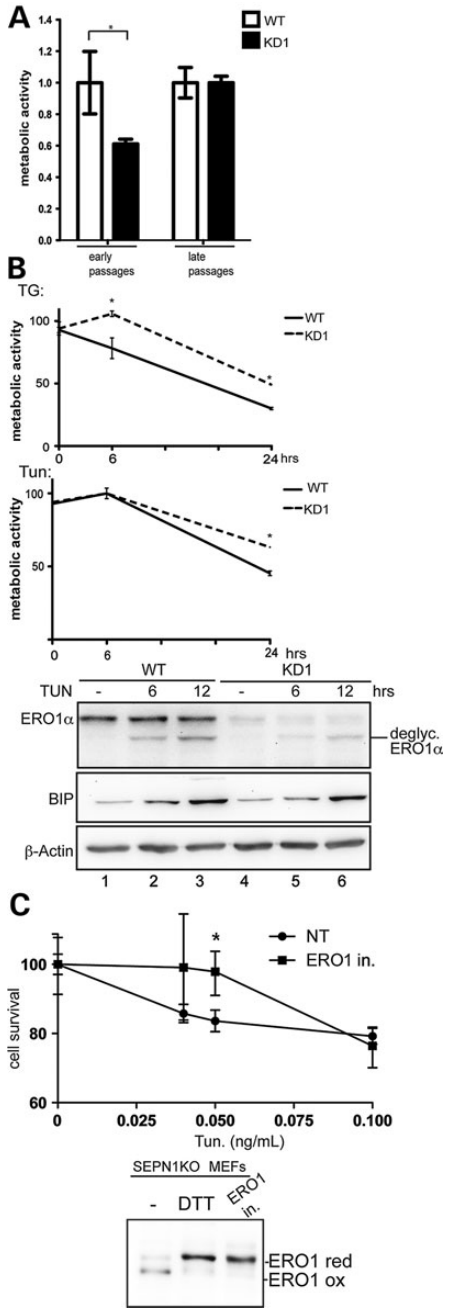

Figure 7. Attenuated ERO1 activity is protective in SEPN1KO cells. (**A**) MTT-dependent metabolic activity of control WT and KD1 cells at early passages (three passages after shRNA lentiviral infection) and late passages (10 passages after the lentiviral infection). The metabolic activity of the WT cells was arbitrarily set at 1 ($n = 6$, $^*P < 0.05$). (**B**) MTT-dependent metabolic activity of control WT and KD1 cells treated with tunicamycin or thapsigargin 10 passages after the lentiviral infection of control or SEPN1-RNAi. Metabolic activity is expressed as the relative amount of MTT in the cells treated with tunicamycin or thapsigargin (the amount of MTT in the untreated cells was arbitrarily set at 100%) ($n = 6$, $^*P < 0.01$). Bottom: immunoblots of endogenous ERO1α BIP and β-actin in lysates of the late passages of WT and KD1 cells exposed to tunicamycin (2.5 mg/ml). (**C**) Survival of SEPN1KO primary MEFs that were untreated or treated with an ERO1 inhibitor (EN460) and subsequently challenged with the indicated concentrations of tunicamycin for 24 h. Survival is expressed as the relative amount of MTT in the cells treated with tunicamycin and the unexposed cells (the amount of MTT in the untreated cells was arbitrarily set at 100%) ($n = 6$, $^*P < 0.05$). Bottom: non-reducing immunoblot of endogenous ERO1α in the lysates of untreated MEFs or MEFs exposed to DTT (10 mM, 30 min) or EN460 (50 μM, 30 min). ERO1ox: oxidized ERO1; ERO1 red: reduced ERO1.

SERCA2b) (Fig. 4) and find that SEPN1 redox-reduces and activates this calcium pumps, consequently enhancing ER calcium loading (Fig. 5).

Moreover, SEPN1 levels parallel those of the protein disulfide oxidase ERO1 suggesting a co-regulation of the two proteins (Fig. 1). Although the underlying mechanisms have not been investigated, this co-regulation suggests that SEPN1 expression may be tuned to attenuate the potentially harmful effects of ERO1 activity.

Indeed, SEPN1 function becomes essential in the case of a hyperoxidized ER elicited by over-expressing ERO1 (Fig. 1) and that, under such conditions, SERCA2 is H_2O_2-oxidized (Fig. 4).

For reasons that are presently unclear, SEPN1KO mice are somehow protected from the effects of SEPN1 loss as they do not show an overt muscle phenotype under usual cage conditions (3,4). We show here that when the muscle level of ERO1 surges as a result of the injection of *ERO1α*-AAV in the gastrocnemius muscle, the fibers develop regions of mitochondrial depletion, known as minicores, which are an hallmark of the phenotype associated with the SEPN1-related myopathies; furthermore, the levels of oxidized glutathione increase. These observations indicate a physiological link between the reductase activity of SEPN1 and the oxidative power of ERO1 (Fig. 6).

In skeletal muscle, SERCA pumps are dominantly responsible for Ca^{2+} reuptake into the sarcoplasmic reticulum (SR) during excitation contraction (EC) coupling. Interestingly, a deficit in SERCA activity leads to a dystrophic muscle, raising cytoplasmic calcium levels with consequent cellular necrosis through calpain activation and formation of mitochondrial permeability transition pore, and adeno-associated virus–SERCA2a (AAV-SERCA2a) gene therapy in the gastrocnemius muscle of *Sgcd*–/– (δ-sarcoglycan–null) mice mitigated the dystrophic phenotype (41).

Our findings therefore suggest a simple scenario, in which the lack of SEPN1 redox activity in an oxidizing environment inhibits SERCA2 activity and thus adversely affects muscle fitness by constitutively enfeebling the machinery for excitation–contraction coupling.

In line with a role of SEPN1 in the regulation of calcium signalling, SEPN1 was found to co-precipitate the calcium release channel RyR (ryanodine receptor) and function as a modifier of this calcium channel (38).

An important question that remains open regards the basis of the muscle-specific pathogenic effect of SEPN1 deficit. We propose that this restriction of damage to skeletal muscle may be linked to the properties of muscle fibres to experience ER stress and produce ROS. Indeed, ER stress is one of the primary processes triggered by altered environmental cues in skeletal muscle. Long-distance running or a simple dietary alteration can activate the ER stress pathway in skeletal muscle, and contracting skeletal muscle produces ROS which, if they are not metabolized, can cause oxidative damage to the macromolecules in muscle fibres (42). Thus, the UPR-mediated up-regulation of ERO1 may cause production of excess of H_2O_2, further aggravating the situation, which must be controlled by counteracting mechanisms (15).

ERO1 activity in mammals is normally counteracted by ER peroxidases such as GPX7, GPX8 and PRDX4, which may use the peroxide generated by ERO1 to introduce another disulfide in new nascent proteins and thus enhance the efficiency of oxidative protein folding (28,43–45). However, it is possible that under certain circumstances and in contracting skeletal muscle the induction of ER peroxidases does not match the excess of H_2O_2 burden produced by ERO1.

At molecular level, the excess of H_2O_2 converts the luminal thiols of the SERCA2 pump into H_2O_2-mediated oxidized derivatives, and the lack of SEPN1 reductase activity (partially compensated by glutathione) traps these thiols in a hyperoxidized state by inhibiting pump activity with a consequent higher level of cytoplasmic calcium and cellular loss.

Thus, while in most circumstances, the transcriptional activation of ERO1 by the UPR is an homeostatic response that increases fitness in some conditions, included the skeletal muscle of SEPN1KO, it may contribute to the maladaptive branch of the UPR. Accordingly, the attenuation of ERO1 activity with the consequent lower level of H_2O_2 provides some protection against the lethality of severe unfolded protein stress in the ER of cells in worms and yeasts and, as shown in this study, cells devoid of SEPN1 (Fig. 7) (23,24).

In conclusion, we have identified SERCA2 isoforms as redox targets of SEPN1, and established that the two cysteines in the L4 domain are involved in the interaction with SEPN1. The interaction between SEPN1 and the isoform of SERCA2 explains the selective hypotrophy of slow-twitch muscle fibres in SEPN1 loss-of-function models, but we cannot exclude the possibility of interactions between SEPN1 and other SERCA. However, regardless of whether there are other redox targets of SEPN1, our findings suggest that the redox interaction between SERCA2 and SEPN1 (together with the previously shown interaction between RyR and SEPN1) regulates calcium levels in the ER, and makes SEPN1 a key component of redox-regulated calcium metabolism. Moreover, our studies linking SEPN1 with ERO1 provide a rationale for using compounds that inhibit or regulate ERO1 activity as potential therapeutic agents in SEPN1-related myopathies (Fig. 8).

Materials and Methods

Animal experiments

All the procedures involving animals and their care carried out at the Mario Negri Institute were conducted as described by the institutional guidelines that are in accordance with national (D.L. no. 116, G.U. suppl. 40, Feb. 18, 1992, No.8, G.U., 14 luglio 1994) and international laws and policies (EEC Council Directive 86/609, OJ L 358, 1 DEC.12,1987; NIH Guide for the Care and use of Laboratory Animals, U.S. National Research Council, 1996). The SEPN1KO mice were purchased from EMMA repository (Sepn1 < tm1.2Mred>/Orl). Genotyping at the *SepN1* locus followed published procedures (3).

Production of AAV vectors

The human *ERO1α* coding with a Myc-tag at C terminal was exchanged with *EGFP* in pAAV2.1 that contains the inverted terminal repeats (ITRs) of AAV serotype 2 and the CMV promoter (46). pAAV2.1-CMV-*ERO1α* and -*EGFP* were used for AAV2/1 vector production. AAV2/1 vectors were produced by the TIGEM AAV Vector Core by triple transfection of HEK-293 cells followed by two rounds of $CsCl_2$ purification. For each viral preparation, physical titers (genome copies-GC/ml) were determined by averaging the titer achieved by dot-blot analysis and by PCR quantification using TaqMan (Applied Biosystems, Carlsbad, CA, USA) (47).

Intramuscular injection of AAV-*ERO1α*, muscle staining

Six 1-month-old WT and six 1-month-old SEPN1KO mice were injected with a total dose of 10^{11}GC of *ERO1α*-AAV2/1 vector

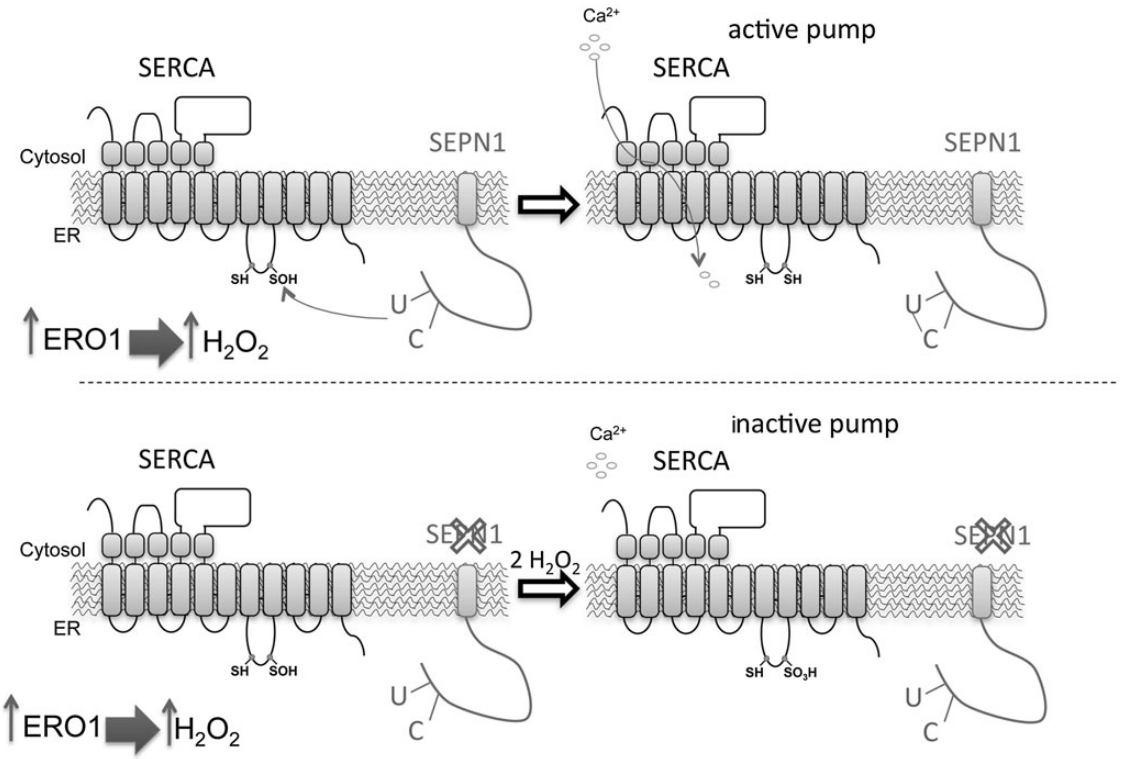

Figure 8. SEPN1 function: a working model. Within the ER, a burst of ERO1 activity (such as that occurring when UPR is elicited) increases the local concentration of H_2O_2, which attacks the luminal thiols in SERCA2 and thus leads to cysteinyl sulfenic acid formation (–SOH). SEPN1 reduces the SOH back to free thiol (–SH), thus restoring SERCA activity. In SEPN1 mutant cells, the unstable cysteinyl sulfenic acid can be further oxidized by one more molecule of H_2O_2 to generate the oxidized sulfenic (–SO_2H), and by two more molecules of H_2O_2 to generate the terminally oxidized sulfonic (–SO_3H) SERCA2. In this oxidized state, SERCA2 is irreversibly inactivated.

preparation in three sites of the right gastrocnemius (three injections of 30 µl each) using a Hamilton syringe. Equivalent doses of AAV2/1CMV-*EGFP* or equal volumes of PBS were injected into the contralateral muscle. The animals were sacrificed 3 weeks after being injected and perfused with PBS. Gastrocnemii, free from neighbouring muscles and connective tissue, were isolated and analyzed. One part of the sample was used to test the level of ERO1α expression by means of western blotting. The muscles were frozen in liquid nitrogen-cooled isopentane, fixed in formalin for morphological analysis and cross sections (8 µm) of isopentane-frozen muscle were stained with hematoxylin and eosin (H&E) for histological evaluation. For the NADH staining, the frozen sections were incubated with nitro-blue tetrazolium (1 mg/ml) and β-nicotinamide adenine dinucleotide (0.4 mg/ml) in 50 mM Tris–HCl (pH 7.3) for 30 min at 37°C.

C2c12, SEPN1 knockdown and lentiviral transduction

C2C12 cells were cultured in DMEM supplemented with 25 mM glucose and 10% fetal calf serum (FCS). SEPN1 was knocked down using Mission™ shRNA-encoding lentiviruses against mouse *SEPN1* mRNA (SHCLND-NM_029100.2, Sigma) following the manufacturer's instructions: knockdown pooled KD1 was targeted with shRNA TRCN0000024786060 and KD2 with TRCN0000247862. Mock cells were obtained by means of a lentivirus driving *puro*-resistance.

Blasticidin resistance-marked lentivirus, pLenti 6.3V5-TOPO (Sigma), which encodes human *ERO1a* was constructed from cDNA donated by Roberto Sitia (DIBIT, Milan, Italy). After transduction and selection with blasticidin at 1 µg/ml for 7 days, the cells (in triplicate wells) were fixed and stained with crystal violet, and the relative cell mass was quantified by solubilising the dye in 0.2% Triton X-100 and measuring absorbance at 590 nm.

SEPN1 expression in eukaryotic cells

Expression plasmids encoding ER-localized and C-terminally FLAG-tagged human *SEPN1* and the related mutants were constructed in pSel-Express vector (a kind gift from Vladimir Gladyshev). The *SEPN1-SS* and *SEPN1-SC* were made by means of QuiKChange site-directed mutagenesis (Stratagene). The cells transfected with *SEPN1* were cultured in the presence of 0.25 mM of sodium selenite in order to allow the expression of full-length SEPN1.

Detecting sulfenic acid-modified proteins in cultured cells

The sulfenic acid-modified proteins were detected using the procedure of Seo and colleagues (27) and immunoblotting using a rabbit serum reactive to sulfenic acid-modified proteins (Millipore).

Isolation and analysis of control and SEPN1KO MEFs

Control and SEPN1 knockout MEFs, isolated at embryonic Day 13.5, were studied as I° MEFs. D^{M} were immortalized with SV-40 large T antigen and cultured in DMEM supplemented to 25 mM glucose, 10% FCS, nonessential amino acids and, where indicated, were exposed to tunicamycin (0.5 µg/ml) and thapsigargin (0.5 mM) (Sigma).

The following I° immunochemical reagents were used: rabbit anti-ERO1α (25), rabbit anti-SEPN1 (Sigma), mouse anti-KDEL (Stressgen), mouse anti-PDI (Stressgen), mouse anti-β-actin (Sigma), mouse anti-SERCA2 (Santa Cruz) and anti-GAPDH (Sigma).

Immunopurification of complexes trapped by SEPN1-FLAG and interaction with SERCA2

Expression plasmids encoding ER localized, C-terminally FLAG-tagged human *SEPN1* were constructed in the pFLAG-CMV1 vector (Sigma). Transfected HEK 293T cells from four confluent 100 mm plates were washed in PBS with 20 mM *N*-ethyl maleimide (NEM), lysed in 0.3% Triton X-100, 150 mM NaCl, 20 mM HEPES, pH 7.4, 20 mM NEM and protease inhibitors. The FLAG-tagged proteins were immunopurified with Flag M2 affinity gel (Sigma) in an overnight incubation and eluted in Lemmli buffer. Ten percent of the eluted material was immunoblotted with anti-FLAG M2 (Sigma) following reducing and non-reducing SDS–PAGE. The co-immunoprecipitation of SEPN1 and SERCA2 was tested on the endogenous SERCA2 or transfected pig *SERCA2b* (pcDNA3), pig *SERCA2a* (pcDNA3) and the mutants pig *SERCA2b2m* (C875S and C887S), pig *SERCA2a2m* (C875S and C887S) that lack the two cysteines in the L4 ER domain and was made by means of QuiKChange site direct mutagenesis (Stratagene). Expression plasmids encoding ER localized *catalase–peroxidase* from Magnaporthe grisea and the catalase mutated in the tryptophan of the active site (W140F) and within frame a ro-GFP-KDEL at C terminal were constructed in pcDNA3 and were a kind gift from David Ron's Laboratory.

Mass spectrometry

The remaining 90% of the eluted material was resolved by means of non-reducing SDS–PAGE and lightly stained with Sypro Ruby. The regions of the gel containing complexes larger than the SEPN1 dimer bait were excised, reduced in 10 mM DTT, alkylated with 20 mM NEM and analyzed by means of mass spectrometry.

Briefly, LC–ESI–MS-MS of 5 µl of each sample was performed on a quadrupole Orbitrap Q-exactive mass spectrometer (Thermo Scientific). Peptides separation was achieved on a linear gradient from 88% solvent A (2% ACN, 0.1% formic acid) to 50% solvent B (80% acetonitrile, 0.1% formic acid) over 20 min and from 50 to 100% solvent B in 2 min at a constant flow rate of 0.25 µl/min on UHPLC Easy-nLC 1000 (Thermo Scientific) where the LC system was connected to a 23-cm fused-silica emitter of 75 µm inner diameter (New Objective, Inc. Woburn, MA, USA), packed in-house with ReproSil-Pur C18-AQ 1.9 µm beads (Dr Maisch Gmbh, Ammerbuch, Germany) using a high-pressure bomb loader (Proxeon, Odense, Denmark).

MS data were acquired using a data-dependent top 10 method for HCD fragmentation. Survey full scan MS spectra (300–1750 Th) were acquired in the Orbitrap with 70000 resolution, AGC target 1^{e6}, IT 120 ms.

For HCD spectra, resolution was set to 17 500 at *m/z* 200, AGC target 1^{e5}, IT 120 ms; Normalized Collision energy 25% and isolation with 3.0 *m/z*. Technical replicates were conducted on the LC–MS-MS part of the analysis. Raw data were processed with MaxQuant version 1.4.05. Peptides were identified from the MS-MS spectra searched against the uniprot_cp_human_2013_11 database using the Andromeda search engine. Cysteine *N*-ethylmaleimide was used as fixed modification, methionine oxidation and protein *N*-terminal acetylation as variable modifications. Mass deviation for MS-MS peaks was set at 20 ppm and a maximum of two missed cleavages was allowed. The peptides and protein false discovery rates (FDR) were set to 0.01; the minimal length required for a peptide was six amino acids; a

minimum of two peptides and at least one unique peptide were required for high-confidence protein identification. The lists of identified proteins were filtered to eliminate reverse hits and known contaminants.

LFQ Intensities of the Ratios SC/SS was normalized by SEPN1 intensity for every conditions.

Statistical *t*-test analysis were done using Perseus program (version 1.4.0.20) in the MaxQuant environment. For all the statistical analysis was applied an FDR 0.05 using a Permutation Test (500 randomizations).

Glutathione content

Tissue and cell levels of total and oxidized glutathione were measured fluorimetrically using the DTNB glutathione reductase recycling assay as described previously (48).

Calcium measurements

HeLa and MEFs cells were grown in Dulbecco's modified Eagle's medium (DMEM) supplemented with 10% FCS in 75 cm^2 Falcon flasks, seeded onto 13 mm glass coverslips and allowed to grow to 50% confluence. At this stage, they were transfected with various constructs using the Ca^{2+} phosphate technique for the HeLa cells or a MicroPorator (Digital Bio) for the MEFs.

In order to obtain efficient reconstitution of the aequorin needed to produce the functional Ca^{2+}-sensitive luminescent protein, the [Ca^{2+}] in the lumen of the store was reduced 36 h after transfection by incubating the cells for 1 h at 4°C in a Krebs–Ringer buffer (KRB: 125 mM NaCl, 5 mM KCl, 1 mM Na_3PO_4, 1 mM $MgSO_4$, 5.5 mM glucose, 20 mM HEPES, pH 7.4) containing 5 μM coelenterazine, the Ca^{2+} ionophore ionomycin and 600 μM EGT. After this incubation, the cells were extensively washed with KRB supplemented with 2% bovine serum albumin (BSA) before measuring the luminescence. After the reconstitution step, the cells were placed in a perfused, thermostated chamber in close proximity to a low-noise photomultiplier with a built-in amplifier/discriminator. The output of the discriminator was captured using a Thorn-EMI photon counting board and stored in an IBM-compatible computer for subsequent analysis. Aequorin photon emission was calibrated off line into [Ca^{2+}] values using a computer algorithm based on the Ca^{2+} response curve of aequorins, as previously described (39,49).

Protein lysate from mouse muscles and mitochondria isolation

The muscles were mechanically disrupted using an Ultra Turrax homogenizer in RIPA buffer. The insoluble material was isolated by means of clarification at maximum speed for 5′ and the lysate was recovered and quantified using the BCA method. The muscles were resuspended in 8 ml mitochondria buffer (70 mM sucrose, 1 mM EGTA, 210 mM sorbitol, 10 mM MOPS, pH 7.4), and crude mitochondria were purified as described in (50). The total proteins and the mitochondrial proteins were quantified using the BCA method.

Statistics

All results are expressed as mean values ± SEM. Two-tailed Student *t*-tests were used to determine *P*-values for paired samples in the case of the experiments involving more than one independent variable.

Supplementary Material

Supplementary Material is available at *HMG* online.

Acknowledgements

We are indebted to David Ron as some reagents were developed in his lab and for the fruitful discussion on the results. We thank Nica Borgese for the comments to our manuscript, Roberto Sitia (Dibit, Milan, Italy) for the human ERO1 plasmid, Vladimir Gladyshev (Harvard Medical School, Boston, USA) for the pselexpress vector, the EMMA repository and Alain Lescure as the provider of the SEPN1 KO mice. The help of Monica Doria (TIGEM AAV Vector Core, Napoli, Italy) for AAV vector production and Sonia Missiroli for carrying out some preliminary experiments is gratefully acknowledged.

Conflict of Interest statement. None declared.

Funding

Supported by a Telethon career award (TDEZ00112T) to E.Z., the Italian Association for Cancer Research (AIRC) and local funds from the University of Ferrara to P.P. and C.G., and from Telethon (GGP11139B) and the Italian Ministry of Education, Universities and Research (COFIN, FIRB and Futuro in Ricerca) to P.P.

References

1. Petit, N., Lescure, A., Rederstorff, M., Krol, A., Moghadaszadeh, B., Wewer, U.M. and Guicheney, P. (2003) Selenoprotein N: an endoplasmic reticulum glycoprotein with an early developmental expression pattern. *Hum. Mol. Genet.*, **12**, 1045–1053.
2. Castets, P., Maugenre, S., Gartioux, C., Rederstorff, M., Krol, A., Lescure, A., Tajbakhsh, S., Allamand, V. and Guicheney, P. (2009) Selenoprotein N is dynamically expressed during mouse development and detected early in muscle precursors. *BMC Dev. Biol.*, **9**, 46.
3. Rederstorff, M., Castets, P., Arbogast, S., Laine, J., Vassilopoulos, S., Beuvin, M., Dubourg, O., Vignaud, A., Ferry, A., Krol, A. *et al.* (2011) Increased muscle stress-sensitivity induced by selenoprotein N inactivation in mouse: a mammalian model for SEPN1-related myopathy. *PLoS ONE*, **6**, e23094.
4. Moghadaszadeh, B., Rider, B.E., Lawlor, M.W., Childers, M.K., Grange, R.W., Gupta, K., Boukedes, S.S., Owen, C.A. and Beggs, A.H. (2013) Selenoprotein N deficiency in mice is associated with abnormal lung development. *FASEB J.*, **27**, 1585–1599.
5. Lacourciere, G.M. and Stadtman, T.C. (1999) Catalytic properties of selenophosphate synthetases: comparison of the selenocysteine-containing enzyme from Haemophilus influenzae with the corresponding cysteine-containing enzyme from Escherichia coli. *Proc. Natl. Acad. Sci. USA*, **96**, 44–48.
6. Arbogast, S., Beuvin, M., Fraysse, B., Zhou, H., Muntoni, F. and Ferreiro, A. (2009) Oxidative stress in SEPN1-related myopathy: from pathophysiology to treatment. *Ann. Neurol.*, **65**, 677–686.
7. Lescure, A., Rederstorff, M., Krol, A., Guicheney, P. and Allamand, V. (2009) Selenoprotein function and muscle disease. *Biochim. Biophys. Acta*, **1790**, 1569–1574.
8. Ashby, M.C. and Tepikin, A.V. (2001) ER calcium and the functions of intracellular organelles. *Semin. Cell Dev. Biol.*, **12**, 11–17.

9. Higo, T., Hattori, M., Nakamura, T., Natsume, T., Michikawa, T. and Mikoshiba, K. (2005) Subtype-specific and ER lumenal environment-dependent regulation of inositol 1,4,5-trisphosphate receptor type 1 by ERp44. *Cell*, **120**, 85–98.
10. Baba-Aissa, F., Raeymaekers, L., Wuytack, F., Dode, L. and Casteels, R. (1998) Distribution and isoform diversity of the organellar Ca2+ pumps in the brain. *Mol. Chem. Neuropathol.*, **33**, 199–208.
11. Li, Y. and Camacho, P. (2004) Ca2+-dependent redox modulation of SERCA 2b by ERp57. *J. Cell Biol.*, **164**, 35–46.
12. Frand, A.R. and Kaiser, C.A. (1998) The ERO1 gene of yeast is required for oxidation of protein dithiols in the endoplasmic reticulum. *Mol. Cell*, **1**, 161–170.
13. Pollard, M.G., Travers, K.J. and Weissman, J.S. (1998) Ero1p: a novel and ubiquitous protein with an essential role in oxidative protein folding in the endoplasmic reticulum. *Mol. Cell*, **1**, 171–182.
14. Sevier, C.S., Qu, H., Heldman, N., Gross, E., Fass, D. and Kaiser, C.A. (2007) Modulation of cellular disulfide-bond formation and the ER redox environment by feedback regulation of Ero1. *Cell*, **129**, 333–344.
15. Gross, E., Kastner, D.B., Kaiser, C.A. and Fass, D. (2004) Structure of Ero1p, source of disulfide bonds for oxidative protein folding in the cell. *Cell*, **117**, 601–610.
16. Tu, B.P. and Weissman, J.S. (2002) The FAD- and O(2)-dependent reaction cycle of Ero1-mediated oxidative protein folding in the endoplasmic reticulum. *Mol. Cell*, **10**, 983–994.
17. Harding, H.P., Zhang, Y., Zeng, H., Novoa, I., Lu, P.D., Calfon, M., Sadri, N., Yun, C., Popko, B., Paules, R. *et al.* (2003) An integrated stress response regulates amino acid metabolism and resistance to oxidative stress. *Mol. Cell*, **11**, 619–633.
18. Powers, S.K., Nelson, W.B. and Hudson, M.B. (2011) Exercise-induced oxidative stress in humans: cause and consequences. *Free Radic. Biol. Med.*, **51**, 942–950.
19. Kim, H.J., Jamart, C., Deldicque, L., An, G.L., Lee, Y.H., Kim, C.K., Raymackers, J.M. and Francaux, M. (2011) Endoplasmic reticulum stress markers and ubiquitin-proteasome pathway activity in response to a 200-km run. *Med. Sci. Sports Exerc.*, **43**, 18–25.
20. Wu, J., Ruas, J.L., Estall, J.L., Rasbach, K.A., Choi, J.H., Ye, L., Bostrom, P., Tyra, H.M., Crawford, R.W., Campbell, K.P. *et al.* (2011) The unfolded protein response mediates adaptation to exercise in skeletal muscle through a PGC-1alpha/ATF6alpha complex. *Cell Metab.*, **13**, 160–169.
21. Ron, D. and Walter, P. (2007) Signal integration in the endoplasmic reticulum unfolded protein response. *Nat. Rev. Mol. Cell Biol.*, **8**, 519–529.
22. Curran, S.P. and Ruvkun, G. (2007) Lifespan regulation by evolutionarily conserved genes essential for viability. *PLoS Genet.*, **3**, e56.
23. Haynes, C.M., Titus, E.A. and Cooper, A.A. (2004) Degradation of misfolded proteins prevents ER-derived oxidative stress and cell death. *Mol. Cell*, **15**, 767–776.
24. Marciniak, S.J., Yun, C.Y., Oyadomari, S., Novoa, I., Zhang, Y., Jungreis, R., Nagata, K., Harding, H.P. and Ron, D. (2004) CHOP induces death by promoting protein synthesis and oxidation in the stressed endoplasmic reticulum. *Genes Dev.*, **18**, 3066–3077.
25. Zito, E., Chin, K.T., Blais, J., Harding, H.P. and Ron, D. (2010) ERO1-beta, a pancreas-specific disulfide oxidase, promotes insulin biogenesis and glucose homeostasis. *J. Cell Biol.*, **188**, 821–832.
26. Kettenhofen, N.J. and Wood, M.J. (2010) Formation, reactivity, and detection of protein sulfenic acids. *Chem. Res. Toxicol.*, **23**, 1633–1646.
27. Seo, Y.H. and Carroll, K.S. (2009) Profiling protein thiol oxidation in tumor cells using sulfenic acid-specific antibodies. *Proc. Natl. Acad. Sci. USA*, **106**, 16163–16168.
28. Zito, E., Melo, E.P., Yang, Y., Wahlander, A., Neubert, T.A. and Ron, D. (2010) Oxidative protein folding by an endoplasmic reticulum-localized peroxiredoxin. *Mol. Cell*, **40**, 787–797.
29. Lohman, J.R. and Remington, S.J. (2008) Development of a family of redox-sensitive green fluorescent protein indicators for use in relatively oxidizing subcellular environments. *Biochemistry*, **47**, 8678–8688.
30. Cuozzo, J.W. and Kaiser, C.A. (1999) Competition between glutathione and protein thiols for disulphide-bond formation. *Nat. Cell Biol.*, **1**, 130–135.
31. Hayes, J.D. and McLellan, L.I. (1999) Glutathione and glutathione-dependent enzymes represent a co-ordinately regulated defence against oxidative stress. *Free Radic. Res.*, **31**, 273–300.
32. Appenzeller-Herzog, C., Riemer, J., Christensen, B., Sorensen, E.S. and Ellgaard, L. (2008) A novel disulphide switch mechanism in Ero1alpha balances ER oxidation in human cells. *EMBO J.*, **27**, 2977–2987.
33. Margittai, E., Low, P., Stiller, I., Greco, A., Garcia-Manteiga, J. M., Pengo, N., Benedetti, A., Sitia, R. and Banhegyi, G. (2012) Production of H(2)O(2) in the endoplasmic reticulum promotes in vivo disulfide bond formation. *Antioxid. Redox. Signal.*, **16**, 1088–1099.
34. Lu, J., Berndt, C. and Holmgren, A. (2009) Metabolism of selenium compounds catalyzed by the mammalian selenoprotein thioredoxin reductase. *Biochim. Biophys. Acta*, **1790**, 1513–1519.
35. Lu, J. and Holmgren, A. (2009) Selenoproteins. *J. Biol. Chem.*, **284**, 723–727.
36. Turanov, A.A., Kehr, S., Marino, S.M., Yoo, M.H., Carlson, B.A., Hatfield, D.L. and Gladyshev, V.N. (2010) Mammalian thioredoxin reductase 1: roles in redox homoeostasis and characterization of cellular targets. *Biochem. J.*, **430**, 285–293.
37. Sandow, A. (1952) Excitation-contraction coupling in muscular response. *Yale J. Biol. Med.*, **25**, 176–201.
38. Jurynec, M.J., Xia, R., Mackrill, J.J., Gunther, D., Crawford, T., Flanigan, K.M., Abramson, J.J., Howard, M.T. and Grunwald, D.J. (2008) Selenoprotein N is required for ryanodine receptor calcium release channel activity in human and zebrafish muscle. *Proc. Natl. Acad. Sci. USA*, **105**, 12485–12490.
39. Bonora, M., Giorgi, C., Bononi, A., Marchi, S., Patergnani, S., Rimessi, A., Rizzuto, R. and Pinton, P. (2013) Subcellular calcium measurements in mammalian cells using jellyfish photoprotein aequorin-based probes. *Nat. Protoc.*, **8**, 2105–2118.
40. Blais, J.D., Chin, K.T., Zito, E., Zhang, Y., Heldman, N., Harding, H. P., Fass, D., Thorpe, C. and Ron, D. (2010) A small molecule inhibitor of endoplasmic reticulum oxidation 1 (ERO1) with selectively reversible thiol reactivity. *J. Biol. Chem.*, **285**, 20993–21003.
41. Goonasekera, S.A., Lam, C.K., Millay, D.P., Sargent, M.A., Hajjar, R.J., Kranias, E.G. and Molkentin, J.D. (2011) Mitigation of muscular dystrophy in mice by SERCA overexpression in skeletal muscle. *J. Clin. Invest.*, **121**, 1044–1052.
42. Rayavarapu, S., Coley, W. and Nagaraju, K. (2012) Endoplasmic reticulum stress in skeletal muscle homeostasis and disease. *Curr. Rheumatol. Rep.*, **14**, 238–243.
43. Tavender, T.J., Springate, J.J. and Bulleid, N.J. (2010) Recycling of peroxiredoxin IV provides a novel pathway for disulphide formation in the endoplasmic reticulum. *EMBO J.*, **29**, 4185–4197.
44. Zito, E., Hansen, H.G., Yeo, G.S., Fujii, J. and Ron, D. (2012) Endoplasmic reticulum thiol oxidase deficiency leads to ascorbic acid depletion and noncanonical scurvy in mice. *Mol. Cell*, **48**, 39–51.

45. Ramming, T., Hansen, H.G., Nagata, K., Ellgaard, L. and Appenzeller-Herzog, C. (2014) GPx8 peroxidase prevents leakage of H2O2 from the endoplasmic reticulum. *Free Radic. Biol. Med.*, **70**, 106–116.
46. Auricchio, A., Hildinger, M., O'Connor, E., Gao, G.P. and Wilson, J.M. (2001) Isolation of highly infectious and pure adeno-associated virus type 2 vectors with a single-step gravity-flow column. *Hum. Gene Ther.*, **12**, 71–76.
47. Colella, P., Trapani, I., Cesi, G., Sommella, A., Manfredi, A., Puppo, A., Iodice, C., Rossi, S., Simonelli, F., Giunti, M. *et al.* (2014) Efficient gene delivery to the cone-enriched pig retina by dual AAV vectors. *Gene Ther.*, **21**, 450–456.
48. Griffith, O.W. (1980) Determination of glutathione and glutathione disulfide using glutathione reductase and 2-vinylpyridine. *Anal. Biochem.*, **106**, 207–212.
49. Pinton, P., Pozzan, T. and Rizzuto, R. (1998) The Golgi apparatus is an inositol 1,4,5-trisphosphate-sensitive Ca2+ store, with functional properties distinct from those of the endoplasmic reticulum. *EMBO J.*, **17**, 5298–5308.
50. Jonassen, T., Marbois, B.N., Faull, K.F., Clarke, C.F. and Larsen, P.L. (2002) Development and fertility in Caenorhabditis elegans clk-1 mutants depend upon transport of dietary coenzyme Q8 to mitochondria. *J. Biol. Chem.*, **277**, 45020–45027.